Topographic Influences on the Wind-Driven Exchange between Marginal Seas and the Open Ocean

HAIHONG GUO[a,b,c] AND MICHAEL A. SPALL[c]

[a] *Key Laboratory of Physical Oceanography, Institute for Advanced Ocean Science, Frontiers Science Center for Deep Ocean Multispheres and Earth System, Ocean University of China, Qingdao, China*
[b] *Pilot National Laboratory for Marine Science and Technology (Qingdao), Qingdao, China*
[c] *Department of Physical Oceanography, Woods Hole Oceanographic Institution, Woods Hole, Massachusetts*

ABSTRACT: The wind-driven exchange through complex ridges and islands between marginal seas and the open ocean is studied using both numerical and analytical models. The models are forced by a steady, spatially uniform northward wind stress intended to represent the large-scale, low-frequency wind patterns typical of the seasonal monsoons in the western Pacific Ocean. There is an eastward surface Ekman transport out of the marginal sea and westward geostrophic inflows into the marginal sea. The interaction between the Ekman transport and an island chain produces strong baroclinic flows along the island boundaries with a vertical depth that scales with the ratio of the inertial boundary layer thickness to the baroclinic deformation radius. The throughflows in the gaps are characterized by maximum transport in the center gap and decreasing transports toward the southern and northern tips of the island chain. An extended island rule theory demonstrates that throughflows are determined by the collective balance between viscosity on the meridional boundaries and the eastern side boundary of the islands. The outflowing transport is balanced primarily by a shallow current that enters the marginal sea along its equatorward boundary. The islands can block some direct exchange and result in a wind-driven overturning cell within the marginal sea, but this is compensated for by eastward zonal jets around the southern and northern tips of the island chain. Topography in the form of a deep slope, a ridge, or shallow shelves around the islands alters the current pathways but ultimately is unable to limit the total wind-driven exchange between the marginal sea and the open ocean.

SIGNIFICANCE STATEMENT: An ocean circulation model and supporting theory are used to understand the wind-driven circulation and exchange through complex ridges and islands between marginal seas and the open ocean. The interaction between the wind-driven flow and island chain produces strong surface-intensified baroclinic boundary currents. The flows between the island are determined by the diffusive balance around the islands, and are characterized by maximum transport in the center of the island chain with decreasing transport toward the southern and northern islands. The topography will alter the current pathways but is ultimately unable to limit the total wind-driven exchange. These results provide a theoretical framework for understanding the circulation around complex islands such as are found in the marginal seas of the western Pacific Ocean.

KEYWORDS: Ekman pumping/transport; Ocean circulation; Topographic effects

1. Introduction

Many previous studies on marginal seas have been able to reproduce the dominant characteristics of the general wind-driven circulation and exchange with the open ocean (Arango et al. 2011; Diansky et al. 2016; Fang et al. 2009; Spall 2002; Stepanov et al. 2018; Yang et al. 2017). In addition to its transport of mass, heat, and salt, this exchange between marginal seas and the open ocean is also important for the regional biological properties (Tang et al. 2004; Wu et al. 2015). Many of these studies focused on the effect of wind stress curl and Ekman pumping (Diansky et al. 2016; Spall 2002; Yang et al. 2017), which are fairly well understood and provide important dynamic mechanisms for the circulation within marginal seas. However, the circulation forced by uniform wind stress is less well studied, although there are indications that it can be important as well. Negative (positive) Ekman transport can enhance (weaken) the Kuroshio intrusion, resulting in strong seasonal variations

of the Kuroshio intrusion (Nan et al. 2015). These studies show that the Ekman transport is important in altering the boundary current through interacting with the coast of a single island. However, we are also interested in the Ekman transport through a more complex geometry with a series of islands and gaps.

The western Pacific Ocean provides many examples of complicated island barriers and bottom topography between marginal seas and open oceans that provide strong dynamical constraints on the circulation. For example, the South China Sea is a large, deep marginal sea that is separated from the Pacific by the Philippine Archipelago, which is characterized by complex topography and a collection of seas connected by many straits and passages (Arango et al. 2011). The Ekman transport contributes significantly to the circulation in and around the Philippine Archipelago region during the monsoon peaks (Han et al. 2009). Theoretical understanding of the circulation around large islands is derived by integrating the momentum equation around a contour that encircles the marginal sea-facing boundary of the island and extends to the

Corresponding author: Haihong Guo, ghh@stu.ouc.edu.cn

coastline of the eastern basin boundary (Godfrey 1989; Pedlosky et al. 1997). This contour integral avoids the western boundary region of poorly known dissipation and ties the throughflow to the wind stress along the contour perimeter by balancing the potential vorticity (PV) flux in this region. Pratt and Spall (2003) developed a porous-medium theory for barotropic flow through complex ridges and archipelagos, in which the throughflows in adjacent gaps are dynamically connected by the circulation integral over a Godfrey contour for each island. Wajsowicz (1996) also extended ''Godfrey's island rule'' to multiple islands to demonstrate that islands separated by narrow gaps are also dynamically connected.

Spatially uniform Ekman transport can produce strong boundary currents around islands. Spall and Pedlosky (2013) provided a general theory for the baroclinic currents both local and remote to the island forced by an Ekman transport toward (away) from the island, even in the absence of wind stress curl. For small islands, nearly all of the approaching Ekman transport flows around the island, however, as the island's meridional extent increases, some amount of this transport will downwell upon encountering the island and flow back in the opposite direction.

The large-scale, low-frequency wind-driven Ekman transport between a marginal sea and the open ocean must be compensated by a flow in the opposite direction, resulting in an exchange between the basins. In the present study, we seek to develop a basic understanding of what determines these exchanges, as well as their dependence on the islands and bottom topography. Numerical model results are first described in section 2, followed by the development of an extended island rule in section 3. Finally, in section 4, a series of diagnostic numerical experiments are carried out to study the effect of topographic shelf and slope or ridge on the circulation and exchange.

2. Numerical model

Understanding the exchange between the marginal sea and an open ocean with an island chain and a topographic ridge located at the mouth of the marginal sea is aided by an idealized numerical model. The advantage of the idealized configuration is that the key characteristics of islands and ridges can be systematically varied in order to test the basic parameter dependencies predicted by the theory developed in the following section. The model is forced by a steady, spatially uniform surface wind stress. While clearly very idealized, this is intended to represent the large-scale, slowly varying monsoon winds in the western Pacific Ocean.

a. Model configuration

The model used in this study is the MITgcm primitive equation model. It solves the primitive equations of motion on a staggered C grid in the horizontal and depth coordinates in the vertical. As shown in Fig. 1a, the domain is 3600 km in zonal extent and 2520 km in meridional extent. The maximum bottom depth is $H = 2000\,\text{m}$. The marginal sea is represented by a relatively small basin extending zonally from the western boundary to $x = 1200\,\text{km}$ and extending from $y = 300\,\text{km}$ to $y = 2220\,\text{km}$ in the meridional direction. The zonal resolution

is 5 km from the western boundary to $x = 2000$ and 20 km from $x = 2000\,\text{km}$ to $x = 3600\,\text{km}$. The meridional resolution is 10 km from the southern (northern) boundary to $y = 900\,\text{km}$ (1620 km) and 2 km from $y = 900\,\text{km}$ to $y = 1620\,\text{km}$. In this example there is an island chain from $y = 920\,\text{km}$ to $y = 1600\,\text{km}$ with a set of small islands and gaps between these islands (the length, width, and number of islands will be varied). The increased model resolution is used to resolve the throughflow in the island gaps. There are 45 levels in vertical, from 10 m over the upper 200 m, and gradually increasing to 200 m at the bottom. The model is forced with a spatially uniform, steady, northward wind stress and run for a period of 6 years with the analysis taken over the average of the final 3 years. The vertical viscosity and diffusion coefficients are 10^{-4} and $10^{-5}\,\text{m}^2\,\text{s}^{-1}$, respectively. We have intentionally chosen to not include a separate mixed layer parameterization that would result in enhanced vertical mixing near the surface resulting from mechanical energy input by the surface wind stress. This allows us to cleanly separate the Ekman layer, which is now entirely contained within the uppermost model level, from the geostrophic flows below the Ekman layer. Additional calculations have shown that the basic results are not sensitive to these mixing parameters. The temperature is restored toward its initial stratification from $x = 2600\,\text{km}$ to the eastern boundary with a time scale of 10 days. This allows us to isolate the marginal sea and island chain from temperature anomalies forced by the interaction of Ekman transport with the eastern boundary.

The key parameters for the example case are as follows: The Coriolis parameter at the southern limit of the domain is $3 \times 10^{-5}\,\text{s}^{-1}$ with meridional variation $\beta = 2 \times 10^{-11}\,\text{m}^{-1}\,\text{s}^{-1}$. The initial stratification $N^2 = 9.81 \times 10^{-6}\,\text{s}^{-2}$. The deformation radius at the midlatitude of the basin is 114 km. The horizontal viscosity is $200\,\text{m}^2\,\text{s}^{-1}$. The wind stress is $\tau = 0.05\,\text{N}\,\text{m}^{-2}$. The zonal extent of the island chain is $L = 35\,\text{km}$. The meridional extent of a single island is $\delta = 28\,\text{km}$ and $\delta_1 = 18\,\text{km}$ for the southernmost and northernmost islands. The meridional width of the gaps is $\Delta = 28\,\text{km}$. The bottom of these gaps is flat without any topographic slope. These parameters will be varied in the following section to test their influence on the circulation around the island chain and topographic influences will be considered in section 4.

b. Example mean circulation

The mean circulation field and density anomaly are shown in Fig. 1. There is an eastward Ekman flow from the marginal sea at the surface and a westward geostrophic flow from the interior of the open ocean below the surface so that the depth integrated zonal flow to the east of the island chain is weak. What is shown in Fig. 1a is the transport in the upper layer that is directly forced by the Ekman transport (240 m, defined in the next section). As the zonal flow encounters the island chain, some of this flow penetrates to the other side through the gaps between the islands, while some downwells along the western side of the islands and returns to the west. There are also enhanced flows around the southern and northern tips of the island chain (Fig. 1). Both the upper-layer throughflow and tip flows are surface intensified and baroclinic. There is also a reversed westward flow through the gaps below the eastward current around the islands, which is much stronger than the
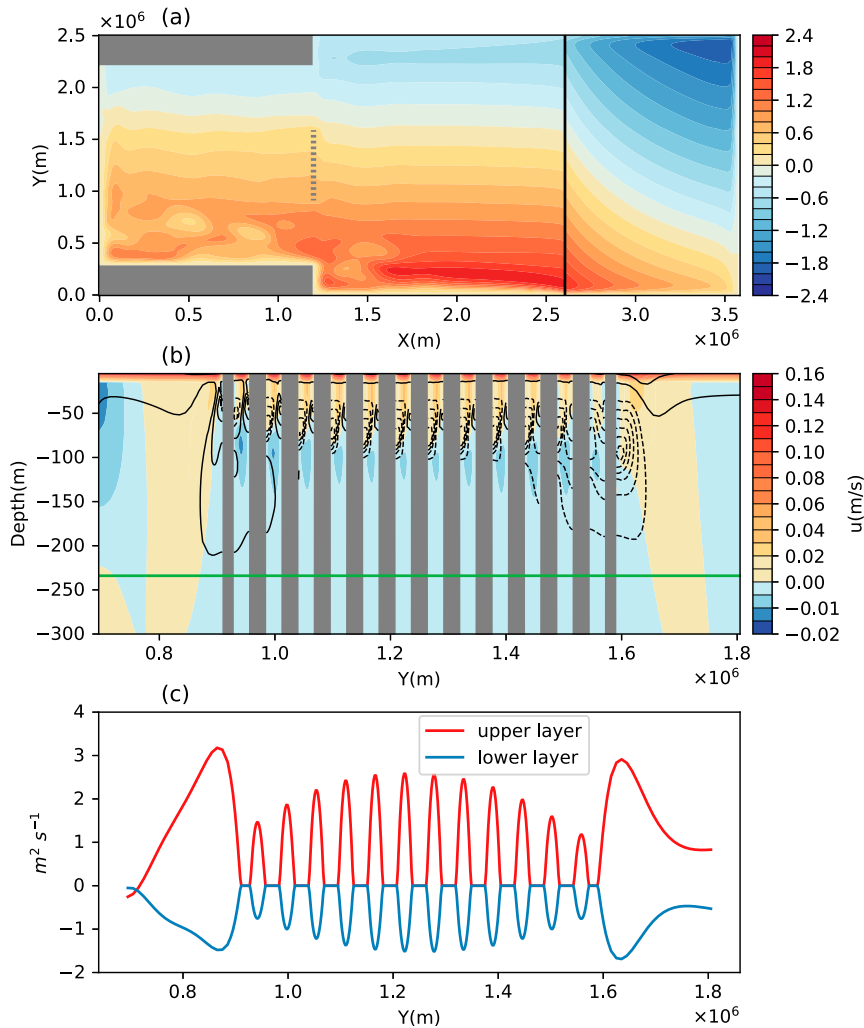
FIG. 1. (a) Vertically integrated transport streamfunction for the upper layer ($D = 240$ m); the black line denotes the western boundary of the temperature restoring region. (b) Vertical section of zonal velocity (color shading) and density anomaly [black contours, the solid (dashed) contours denote positive (negative) anomaly and the contour interval 0.01 kg m^{-3}] at the midlongitude of the island chain. The green line denotes the bottom of the upper layer, as defined by (2) in the text. (c) Vertically integrated zonal velocity of upper and lower layers.

geostrophic flow that comes from the open ocean interior (Fig. 1b). The reversed flow is also geostrophic but associated with the warm and cold anomalies in the thermal boundary layer, which is dynamically different from the weak westward geostrophic flow in the interior that is controlled by the meridional gradient in sea surface height (Spall and Pedlosky 2013). These westward flows are akin to the deep counter currents that are forced by Ekman upwelling at a coast (Yoshida 1980; Suginohara 1982; McCreary et al. 1987).

3. Theory

a. The vertical structure

A simple estimate for the vertical scale of the baroclinic current resulting from the interaction of the Ekman

transport with the boundary can be derived through consideration of the quasigeostrophic potential vorticity q for the flow below the Ekman layer, where ψ is the velocity streamfunction:

$$q = \nabla^2 \psi + \beta y + \frac{f_0^2}{N^2}\frac{\partial^2 \psi}{\partial z^2}. \tag{1}$$

The vertical scale of the baroclinic flow D can be estimated directly from (1) by considering a balance of the terms on the right-hand side. The streamfunction ψ is scaled with the velocity of the fluid drawn into the Ekman layer, $\psi = y\tau/\rho_0 f_0 D$. It is assumed that the relative vorticity and stretching vorticity are of similar magnitude, so that the horizontal length scale of the boundary current scales as ND/f_0. The vertical length scale is then derived directly from (1) to be
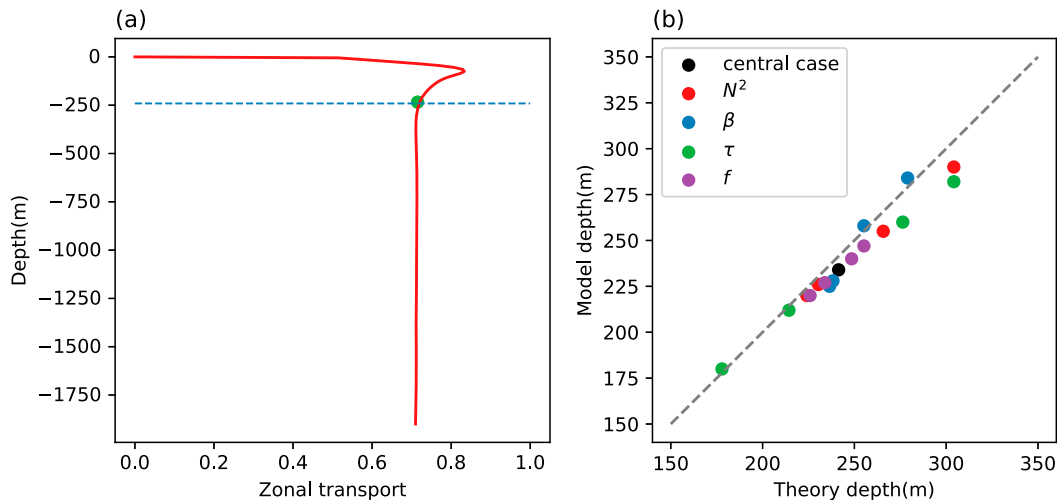
FIG. 2. (a). The vertically integrated throughflow in the gaps from the surface to each depth (red line) for the central case. The blue dashed line denotes the vertical scale predicted by (2), and the green dot denotes the vertical scale diagnosed in the model. (b) Comparison of vertical length scale between model and theory for the series of calculations in Table 1.

$$D = \left(\frac{\tau f_0}{\rho_0 N^2 \beta}\right)^{1/3} = H\left(\frac{L_I}{L_d}\right)^{2/3}. \qquad (2)$$

The inertial boundary layer $L_I = (U/\beta)^{1/2}$, where $U = \tau/\rho_0 f_0 H$ is the Ekman transport distributed over the full depth of the basin H and the baroclinic deformation radius $L_d = NH/f_0$. This scaling demonstrates that the vertical scale of the boundary current depends not only on the stratification, but also on the strength of the wind forcing, the Coriolis parameter, and β.

We use this depth scale D to distinguish the upper-layer boundary current directly forced by the interaction between the Ekman transport and lateral boundary from the deeper geostrophic flows that come from the ocean interior. According to (2), the vertical scale at the midlatitude of the island chain is 240 m for this case. Figure 1c shows the vertically integrated zonal velocity at the midlongitude of the island chain for the upper-layer (lower-layer) flows are shallower (deeper) than this depth. There is eastward flow in the upper layer and westward flow in the lower layer through the gaps and around the tips of the island chain. Interestingly, both the upper-layer flow and the lower-layer flow have the maximum transport in the middle gap and a gradually decreasing throughflow in the gaps to the south and north of the middle gap.

Because the problem is linear and there is no upwelling at depth D, we may consider the upper-layer and lower-layer flow separately. The lower-layer geostrophic flow is nearly barotropic and is quite weak compared to the upper-layer flow. However, the upper-layer flow is not uniformly eastward but is instead surface intensified with a westward flow below (Fig. 1b). To clearly distinguish the flow forced by the interaction of the Ekman layer with the island from that resulting from the westward barotropic return flow, we set a

20-m-depth ridge 100 km to the east of the island chain, between $y = 700$ km and $y = 1820$ km. This blocks the lower-layer geostrophic flow from impinging on the island chain from the eastern open ocean but allows the surface Ekman flow to pass. Therefore, there will be an upper-layer flow that is unaffected by the shallow ridge to the east of the island chain, but there is no deep westward flow in the interior over the latitude range of the island chain. The key parameters of this central case are identical to those in the example in Fig. 1 except for the shallow ridge.

The vertically integrated zonal transport across all the gaps within the latitude band of the islands from the surface to each depth for the central case is shown in Fig. 2a (this does not include the tip flows). The throughflow is scaled by the Ekman transport within the range of latitude from the southern tip of the island chain to its northern tip. The total transport fraction increases from the surface to approximately 100-m depth with a maximum transport fraction of 0.83. Because of the reversed flow below the eastward flow, the transport decreases from the maximum transport to the bottom of the upper layer so that the depth integrated transport of 0.71 is a little weaker than the maximum transport. Therefore, the island chain has blocked almost 30% of the Ekman transport within the latitude band of the islands. We diagnose the vertical scale of the throughflow from the model fields by taking the depth below the maximum transport depth at which the throughflow transport is within 2% of its full depth-integrated transport. The vertical scale in the model is 234 m for the central case, which is quite close to the theoretical prediction (240 m). They are indicated in Fig. 2a by the green dot (model) and the blue dashed line (theory).

To further test the parameter dependence predicted by (2), the wind stress, stratification, f_0, and β were all varied from the central case used here, as summarized in Table 1. The vertical scale diagnosed from the model is compared to the scaling

TABLE 1. The summary of the model runs with key parameters for the diagnostic of the vertical scale.

Run	f_0 (10^{-5} s^{-1})	β (10^{-11} m^{-1} s^{-1})	τ (N m^{-2})	N^2 (10^{-6} s^{-2})
Central case	3	2	0.05	9.81
1	2	2	0.05	9.81
2	2.5	2	0.05	9.81
3	3.5	2	0.05	9.81
4	4	2	0.05	9.81
5	3	1	0.05	9.81
6	3	1.5	0.05	9.81
7	3	2.15	0.05	9.81
8	3	2.25	0.05	9.81
9	3	2	0.02	9.81
10	3	2	0.035	9.81
11	3	2	0.075	9.81
12	3	2	0.1	9.81
13	3	2	0.05	4.91
14	3	2	0.05	7.36
15	3	2	0.05	11.3
16	3	2	0.05	12.3

predicted by (2) in Fig. 2b. In general, there is a good agreement for each of the sets of parameter variations. The vertical length scale varies between about 175 and 300 m. The vertical scale of the upper-layer flow is small for high stratification, weak winds, small Coriolis parameter, and large β. The offshore Ekman transport on the eastern side of the island chain is balanced by the onshore Ekman transport on the other side of the island through the boundary currents in the gaps and the geostrophic flows around the tips of the island chain within this upper layer. Far to the east of the islands this eastward transport is once again carried entirely within the Ekman layer.

b. Exchange through the archipelago

The throughflow in the gaps in the previous example is less than the Ekman transport approaching the island chain from the west because of blockage by the islands. We now derive a theory to understand how much of the flow is blocked by the islands through the application of an extended island rule. We apply the theory to the upper-layer flow without loss of applicability for the lower layer because the theory is linear so it does not matter which direction the flow is going. The same approach could be applied to a zonal flow interacting with a gappy ridge in the deep ocean.

A key assumption of the island rule (Godfrey 1989) is that the frictional dissipation of vorticity around the island is assumed to occur primarily on its eastern side of the island. However, there also exist boundary layers along the southern and northern boundaries for a zonally elongated island (Pedlosky et al. 1997; Pratt and Pedlosky 1998; Spall 2002). Therefore, there are three diffusive boundary layers for each individual island in the island chain: the eastern side boundary scaled by the Munk boundary layer width $\delta_M = (A_h/\beta)^{1/3}$ and the meridional boundary layers on the northern and southern sides of the island whose width scales as $l_m = \delta_M^{2/4} x^{1/4}$ (Pedlosky et al. 1997; Pratt and Pedlosky 1998; Spall 2002).

There are two boundary layers within each gap: one along the northern boundary of the southern island and one along the southern boundary of the northern island. The throughflow will begin to be blocked if the width of the gaps is narrower than approximately 2 times the meridional diffusive boundary layer width.

To study the detailed throughflow, we apply the island rule on each individual island. Following Pedlosky et al. (1997), the starting point of the extended island rule is the integration of the tangential component of the depth-integrated linear momentum equation around the nth island (contour Γ in Fig. 3):

$$\frac{\partial}{\partial t} \oint_\Gamma D\mathbf{u} \cdot \mathbf{s}\, ds + \oint_\Gamma Df\mathbf{k} \times \mathbf{u}\, ds = -D\oint_\Gamma \nabla\left(\frac{p}{\rho}\right) ds + DA_h \oint_\Gamma \nabla^2 \mathbf{u}\, ds + \oint_\Gamma \frac{\tau}{\rho} \cdot \mathbf{s}\, ds, \quad (3)$$

where $\mathbf{u}$ is the mean horizontal velocity in the upper layer, A_h is the lateral viscosity coefficient, D is the thickness of the upper layer given by (2), $\mathbf{s}$ is the unit tangent vector to the contour Γ, τ is the wind stress, p is the pressure, and ρ is the density. Since the wind stress is spatially uniform, the tangential component of the total vorticity flux vanishes around the island, and the pressure term also vanishes around a closed contour, the integral balance of the steady flow is between the dissipation along the eastern, northern, and southern boundaries of the island.

Following Pedlosky et al. (1997), the mean meridional transport along the eastern boundary (T) scales as $V\delta_M D$, where V is the scaling of the meridional velocity along the eastern side boundary. We also assume a boundary layer scaling such that the length scale perpendicular to the boundaries is much less than the length scale along the boundaries. The contribution to the dissipation integral along the eastern side boundary is then approximated by

$$\int DA_h \frac{\partial^2 v}{\partial x^2} dy \sim \frac{A_h T \delta}{\delta_M^3}. \quad (4)$$

The transport T can be represented by $T = (T_{n-1} + T_n)/2$ for the nth island (Fig. 3), and δ is the meridional extent of a single island. The same scaling results if, following Godfrey (1989), we extend the contour integral all the way to the eastern boundary of the basin.

For the meridional boundary layers, if the gap is narrower than 2 times the meridional diffusive boundary layer ($\Delta < 2l_m$), the contribution to the dissipation integral along the meridional boundary can be approximated by

$$DA_h \oint_{\Gamma_n} \frac{\partial^2 u}{\partial y^2} ds = \frac{DA_h L}{2}\left[\frac{u_{n-1}}{(\Delta/2)^2} - \frac{u_n}{(\Delta/2)^2}\right] = 8A_h L\left(\frac{Q_{n-1}}{\Delta^3} - \frac{Q_n}{\Delta^3}\right). \quad (5)$$

Parameter Q_n denotes the transport through the nth gap and we have assumed that the velocity decreases from $2u$ at the center of the gap to 0 at the boundaries.

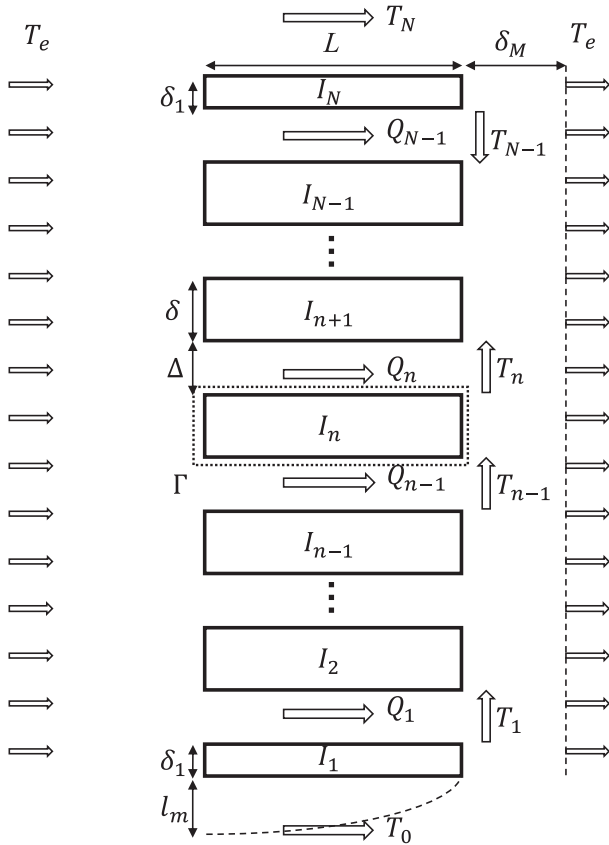Combining (4) and (5), (3) can be written for gap n as

FIG. 3. Definition sketch for the island chain with eastward throughflows. The circulation integral taken around each island is indicated by the dotted contour Γ for island n; T_n and Q_n are the meridional and zonal transports in the vicinity of the islands, and T_e is the Ekman transport.

$$8L\left(\frac{Q_{n-1}}{\Delta^3} - \frac{Q_n}{\Delta^3}\right) + \frac{(T_{n-1} + T_n)\delta}{2\delta_M^3} = 0. \tag{6}$$

The transport around the tips of the island chain is carried in boundary currents that scale with the baroclinic deformation radius L_d, so that the velocity at the southern tip is scaled by T_0/DL_d, where T_0 is the transport around the southern tip. The circulation integral for the first island may be written as

$$\frac{LT_0}{L_d l_m^2} - 8L\frac{Q_1}{\Delta^3} + \frac{(T_0 + T_1)\delta_1}{2\delta_M^3} = 0. \tag{7}$$

A similar expression is derived for the northernmost island (the Nth island in Fig. 3):

$$-\frac{LT_N}{L_d l_m^2} + 8L\frac{Q_{N-1}}{\Delta^3} - \frac{(T_{N-1} + T_N)\delta_1}{2\delta_M^3} = 0. \tag{8}$$

Since the Ekman flux on the eastern side of the island is ultimately fed by the Ekman flow on the western side (Spall and Pedlosky 2013; Pedlosky 2013), the vertically integrated zonal transport of the upper layer on the eastern and western
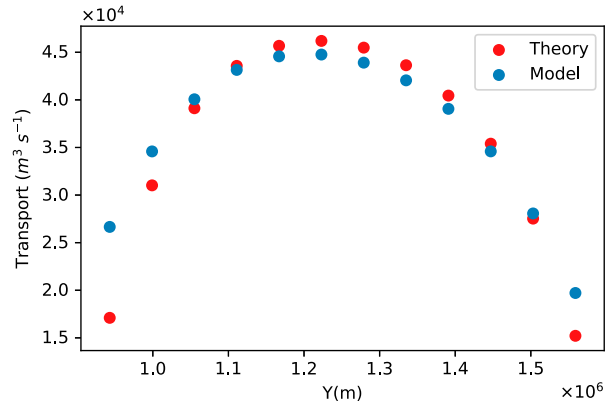

FIG. 4. A comparison between the throughflow in the model (blue) and it is predicted by the theory (red) for the central case.

side of the island chain should balance each other. Recall that there is no upwelling or downwelling through depth D, so the mass balance is closed by lateral fluxes only. The sum of the throughflow in the gaps and the flows around the southern and northern tips of the island chain must be equal to the eastward Ekman transport to the east of the island within the latitude range of the island chain, which provides another equation,

$$T_0 + Q_1 + \cdots + Q_n + \cdots Q_{N-1} + T_N = T_e[(N-2)(\delta + \Delta) + \Delta + 2\delta_1], \tag{9}$$

where $T_e = \tau/\rho_0 f$ is the Ekman transport per unit meridional distance.

The coupled set of Eqs. (6)–(9) form a system of equations with $N+1$ equations and $N+1$ unknowns: T_0, Q_1, Q_2, … Q_{N-1}, and T_N, which can be readily solved. Therefore, the throughflows in the gaps are determined by balancing the diffusion around each island. Because the transport through each of the narrow gaps acts on two islands, the flow through each gap is dependent on the flow through every other gap, similar to the porous medium theory of Pratt and Spall (2003).

The throughflow in each gap in the model for the central calculation compares well with the strength predicted by the diffusive balance theory (Fig. 4). The theory reproduces the magnitude and key features of the model throughflow, including that the transport increases from the tips of the island chain toward the middle. The throughflow is a little asymmetric, with stronger throughflow across the southern portion of the island chain than its northern portion due to the meridional variation in the Coriolis parameter. While for a single island with a small meridional extent the β effect can be neglected, for the whole island chain the variation of the Coriolis parameter leads to a stronger Ekman transport and a stronger throughflow at the lower latitudes.

The transport through the gaps is less than the Ekman transport approaching the islands from the west. The Ekman transport that does not flow through the gaps downwells along the western side of the island over vertical scale D and flows back toward the west. Nonetheless, the Ekman transport on

TABLE 2. The summary of the model runs with key parameters for the diagnostic of the total throughflow fraction.

Run	β ($10^{-11}\,\mathrm{m}^{-1}\,\mathrm{s}^{-1}$)	A_h ($\mathrm{m}^2\,\mathrm{s}^{-1}$)	δ (km)	Δ (km)	L (km)	l_m (km)
Central case	2	200	28	28	35	24.3
1	1	200	28	28	35	28.9
2	2.25	200	28	28	35	23.6
3	2	50	28	28	35	17.2
4	2	400	28	28	35	28.9
5	2	200	16	28	35	24.3
6	2	200	40	28	35	24.3
7	2	200	28	16	35	24.3
8	2	200	28	40	35	24.3
9	2	200	28	28	15	19.7
10	2	200	28	28	55	27.2

the eastern side of the island chain still requires the same transport as is approaching from the west. The difference is supplied by the flow around the tips of the island chain. Thus, the islands result in an overturning cell that is confined within the marginal sea, and they alter the flow pathways in the marginal sea, but they do not alter the net exchange between the marginal sea and the open ocean.

The maximum throughflow in the middle of the island chain is easy to understand from the circulation integral. The flow around the southern end of the island chain will turn northward along the eastern side of the islands. The eastern boundary current on the southern portion will move northward ($T > 0$), which results in a positive contribution from the eastern side boundary to the circulation integral around the island (3). Therefore, there must be a negative contribution from the meridional boundary layer. Since the throughflow in the southern gap provides a positive contribution to the diffusion integral, the throughflow in the northern gap must be stronger than it is in the southern gap ($Q_n > Q_{n-1}$). A similar argument applies to starting at the northern end of the island chain, resulting in the maximum throughflow at the center of the island chain.

It is instructive to write the circulation integrals (6), (7), and (8), in the nondimensional form where, for simplicity, the baroclinic deformation radius and the Ekman transport are assumed to be constant with latitude. This introduces a slight distortion for very long island chains but does not change the fundamental parameter dependencies:

$$Q_n = Q_{n-1} + R(T_n + T_{n-1}), \quad (10a)$$

$$T_0(1 + \gamma RC) = CQ_1 - \gamma RCT_1, \quad (10b)$$

$$T_N(1 + \gamma RC) = CQ_{N-1} - \gamma RCT_{N-1}. \quad (10c)$$

The ratio of the length of the end islands to the middle islands is $\gamma = \delta_1/\delta$.

There are two key nondimensional parameters that control the circulation through the archipelago and determine how much flow is blocked by the islands. The first is the ratio of the geometric factors contributing to the dissipation integral on the eastern boundary of the island to that on the northern and southern boundaries of the island (Pedlosky et al. 1997):

$$R = \frac{\Delta^3 \delta}{16 L \delta_M^3}. \quad (11)$$

This emphasizes the importance of the width of the gaps compared to the Munk layer thickness. This parameter is also proportional to the ratio of the throughflow difference between the adjacent gaps to the boundary current transport along the eastern side of the island chain. We are interested in cases where $O(R) \ll 1$ and frictional blocking of the flow is expected to occur. Pedlosky et al. (1997) got a similar parameter for a single zonally elongated island near the northern boundary with a narrow gap.

The second nondimensional parameter is the ratio of the geometric factors for the dissipation along the gap side of the southern and northern ends of the island chain to the dissipation along the northern or southern tip of the island,

$$C = \frac{8 L_d l_m^2}{\Delta^3} = \frac{8 L_d \delta_M^{3/2} L^{1/2}}{\Delta^3}. \quad (12)$$

The measure of the relative importance of the southern and northern tip boundary to the eastern boundary of the first and last islands is given by RC. While R is typically small, $C \gg 1$ if the gap width is small compared to the baroclinic deformation radius and the Munk layer. For $RC \gg 1$ dissipation on the southern tip is small and the flow through the first gap is balanced by dissipation along the eastern boundary. In that case, the flow through the first gap $Q_1 \approx R(T_0 + T_1)/2$ and the throughflow is independent of C. If $RC \ll 1$ then dissipation along the southern boundary dominates that along the eastern boundary of the island and $Q_1 \approx T_0/2C$. In these cases, the flow through the first gap is much less than the flow around the southern tip of the island. The change in flow between adjacent gaps is proportional to $R \ll 1$ and so the cumulative flow through the gaps is also much less than the transport around the southern tip of the island chain. In this limit the islands are effective at blocking the Ekman transport from passing through the gaps.

A series of 10 additional model calculations have been carried out with varied β, A_h, island length, gap width, and island width in order to demonstrate the dependence of the throughflow on R, as summarized in Table 2. Figure 5 shows the maximum throughflow scaled by the Ekman transport within the latitude band of the central island and gap as a function of R diagnosed
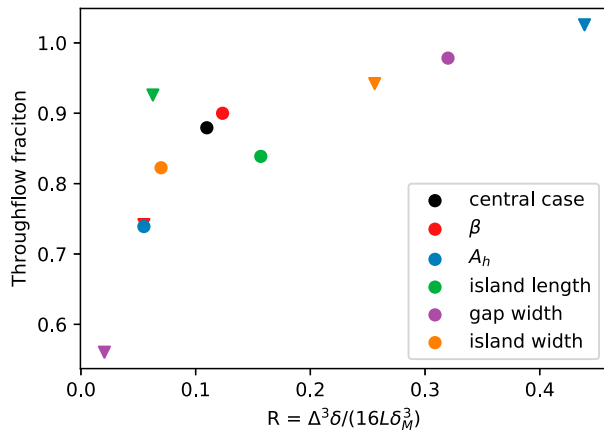
FIG. 5. The throughflow of the gap with the maximum transport scaled by the Ekman transport within the latitude band of the island chain as a function of R. The dots denote the varied parameters are larger than the central case, and the triangles denote the varied parameters are smaller than the central case.

from the model runs in Table 2. The maximum throughflow is clearly reduced for $R \ll 1$. Stronger viscosity or smaller β will lead to a wider Munk boundary layer on the eastern side of the island that requires stronger eastern boundary flows, stronger tip flows, and less throughflow. Stronger viscosity in the meridional boundary layers occurs for a wider Munk layer, narrower gap, or larger zonal extent of the island, which blocks more throughflow. The throughflow fraction does not scale with R for the cases in which the island length is varied (green symbols), pointing to the importance of not only on the flow in a single gap but also on the number of gaps.

The throughflows depend on the width of the gaps, the length and width of the islands, and the thickness of the Munk boundary layer. Figure 6a shows the throughflow comparison between the 10 model runs in Table 2 and the theory for each gap. The agreement between the throughflow diagnosed from the model and that predicted by the diffusive balance theory is quite good. This includes both the sensitivity of the overall throughflow to the model parameters but also the difference in the flow through each gap for each set of parameters.

The parameter dependence of the tip flows predicted by the theory is also reproduced by the model (Fig. 6b). This confirms the assumption that the tip flows compensate for the flow blocked by the islands. The parameter dependence shows that the tip flows are stronger for smaller β, stronger viscosity, narrower gaps, and wider islands. In each of these cases, the flow through the gaps is reduced, there is more downwelling along the western side of the islands, and thus more transport is drawn from the western basin in zonal jets that flow around the tips of the island chain.

A similar porous-medium theory for barotropic flow through ridges and archipelagos has been provided by Pratt and Spall (2003). They considered a uniform negative wind stress curl which produces a uniform, southward meridional Sverdrup flow. As this flow encounters a set of zonal elongated islands or ridges with narrow straits to the south and north of each island, the impinging flow on the northern boundary will split and flow eastward and westward about a stagnation point. Because of the porosity, the circulation integral over a Godfrey-like contour for each of the bumps or islands requires zonal throughflow in the gaps near the southern (northern) boundary, which depends on the porosity and zonal width of the islands. It is noteworthy that
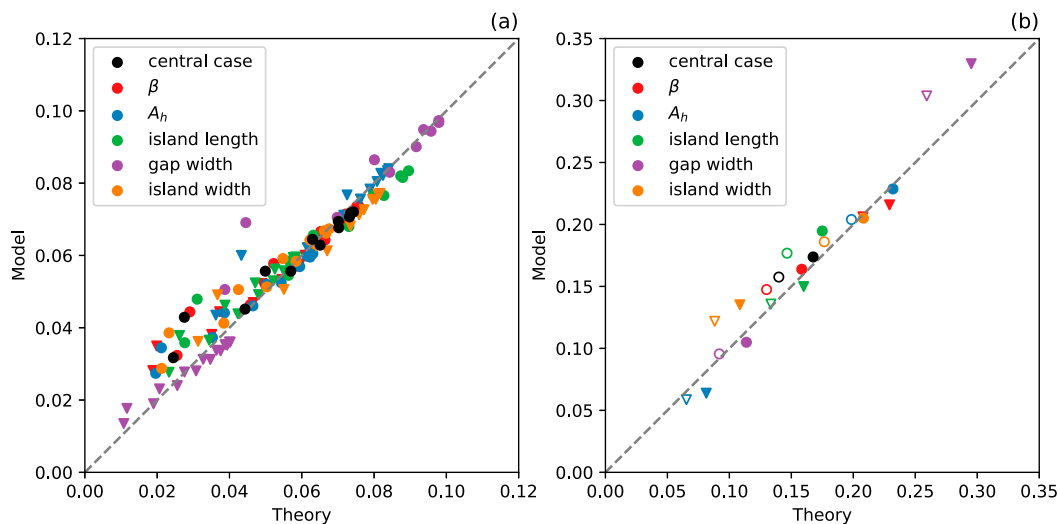

FIG. 6. (a) Comparison of the throughflow in each gap between the model and the theory. The black dots denote the central case, the colored dots denote the parameter variation diagnostic shown in Table 2. The dots denote the varied parameters are larger than the central case, and the triangles denote the varied parameters are smaller than the central case. (b) As in (a), but for the tip flows, the solid markers represent the southern tip flow, while empty markers represent the northern tip flow. All these flows are scaled by the Ekman transport within the latitude band of the island chain.
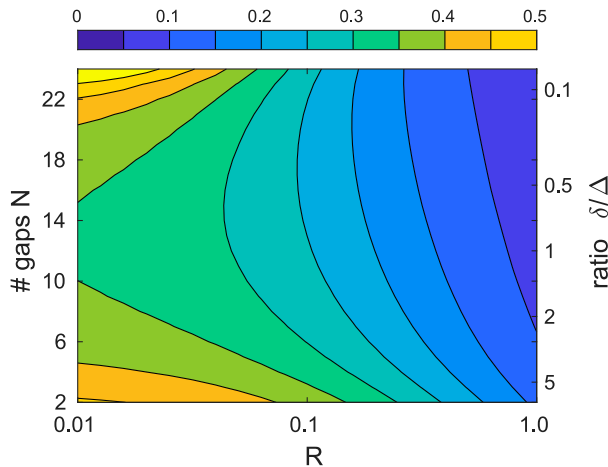
FIG. 7. Amount of Ekman transport blocked by the island chain as a function of R and the number of gaps in the island chain. The total length of the island chain and the gap width Δ are fixed. The number of gaps can also be represented as the ratio of the island length to the gap width (right-hand axis).

FIG. 8. The vertically integrated streamfunction of the upper layer. The white line denotes the shallow ridge.

both Pratt and Spall (2003) and our theory demonstrate that the throughflow in a single gap is not determined locally, but depends on the throughflow in adjacent gaps. However, the structure of the throughflow is very different under their meridional background flow. The uniform impinging meridional flow produces an end effect with the strongest throughflow located in the southernmost (northernmost) gap and weaker throughflow toward the middle of the ridge system (Pratt and Spall 2003). The present uniform impinging zonal flow results in a maximum throughflow at the midlatitude and decays toward the tips.

A fundamental quantity of interest in the amount of the Ekman transport that is blocked by the islands. This depends not only on R but also on the length of each island (or the number of gaps between the islands). We now solve the nondimensional equations (10) as a function of R and the number of gaps. In each case, the total length of the island chain and the width of the gaps between adjacent islands are fixed and either R or the number of islands (or the island length δ) are changed. The fraction of the total Ekman transport approaching the islands from the west that is blocked by the islands is shown in Fig. 7. The y axis is labeled as either the number of gaps on the left or the ratio of the island length to the gap width on the right. For intermediate numbers of gaps, so that $\delta/\Delta = O(1)$, the throughflow is relatively insensitive to the number of islands. As expected, the blocking increases as R decreases, as previously discussed. The blocking increases for fewer gaps, which is not surprising since more of the island chain is a solid boundary. The blocking exceeds 40% for $R = 0.01$ and only two gaps. More surprising is that as there are lots of narrow islands, so that $\delta/\Delta \ll 1$, the blocking also increases, even though a larger fraction of the island chain is represented by open water. This is because as the islands get smaller there is less eastern boundary to balance the viscosity along the northern and southern boundaries. To balance the circulation integral, the transport along the eastern
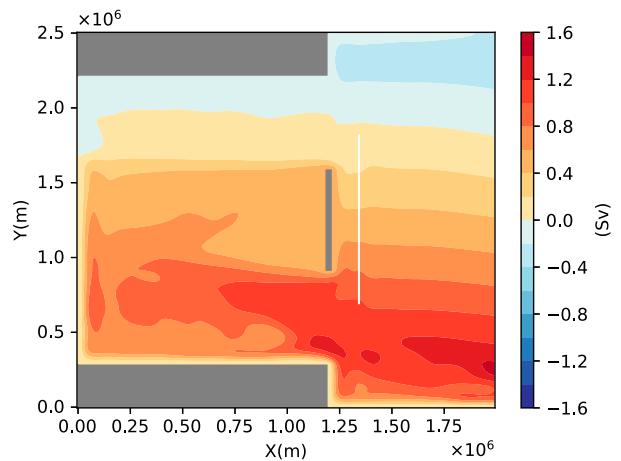
boundary increases and the transport through the gaps decreases. This effect is only found for $R \ll 1$ because that is when friction in the gaps is large.

In the limit of a single very narrow, long island, like the island of Japan between the Japan/East Sea and the northwestern Pacific Ocean, the dissipation on the northern and southern boundaries is not sufficient to balance a unidirectional flow along the eastern boundary. In these cases, the diffusion on the eastern side of the island chain will balance itself, which means there will be both northward and southward flows and a stagnation point along the eastern boundary (Pedlosky et al. 1997). An example of such a case is shown in Fig. 8. In this case, the upper-layer transport west of the island is nearly zero. There is still an eastward Ekman transport but it is now balanced by a westward flow below the Ekman layer but above depth D. The long island supports downwelling on its western side, which feeds a westward flow in the upper layer and results in a local overturning circulation to the west of the island. However, the Ekman transport east of the island still requires the same transport. There is no way for this to be fed from the east because the information in this linear system propagates from east to west. The pressure signal on the island propagates westward, forming discontinuities at the latitudes of the northern and southern tips of the island. This drives zonal jets that extend from the western boundary to the tips of the island and that supply the offshore Ekman transport on the eastern side of the island.

4. Topographic effects

The structure of the throughflow in the island chain is well predicted by the baroclinic boundary scaling estimate and the diffusive balance theory in a flat bottom ocean. Bottom topography can be very important for isolating the island and the marginal sea from geostrophic flows in the ocean interior by modifying potential vorticity contours. We consider three types of topography: a deep topographic slope encircling the island chain, a shallow shelf with a continental slope to the
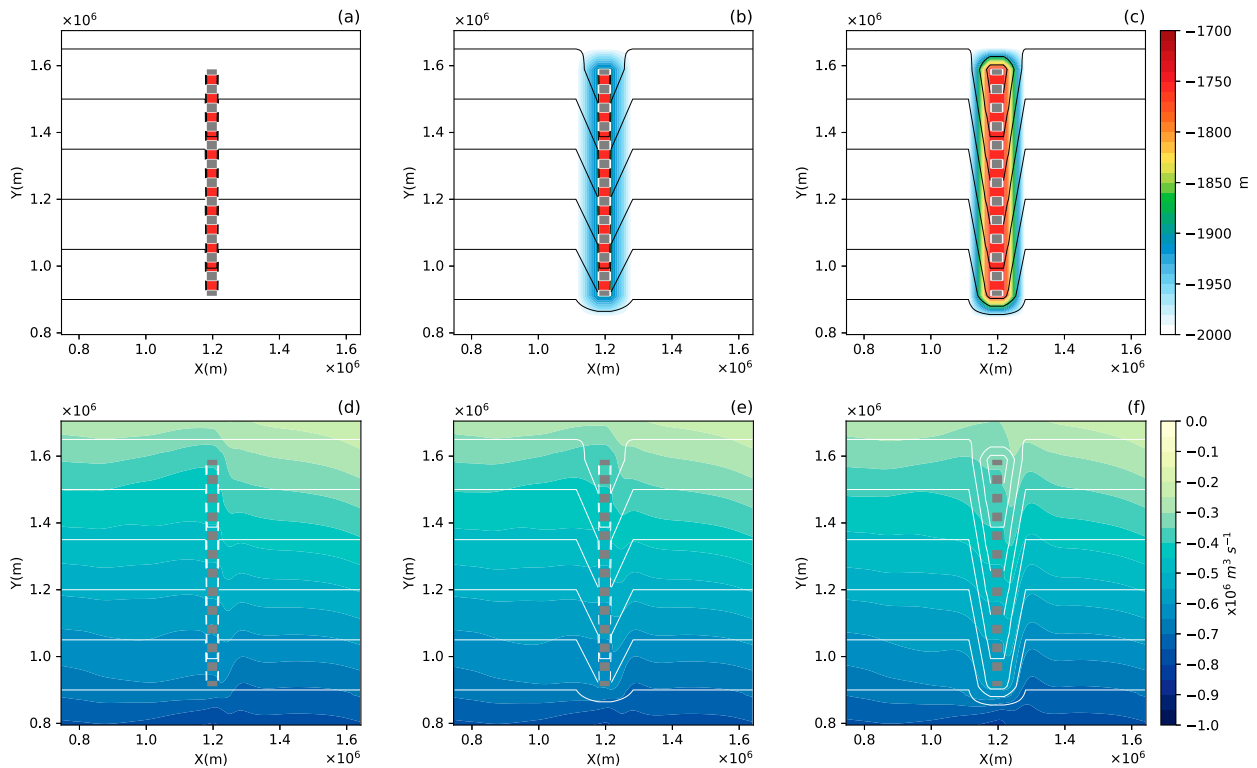
FIG. 9. (a) The topography of the experiments with 1750-m-depth flat ridges in the gaps for the flat bottom ocean and topographic skirt around the island chain whose depth extends to (b) 1900 m ($\alpha = 2.1$) and (c) 1750 m ($\alpha = 5.3$) to flat bottom. (d)–(f) The vertically integrated streamfunction of the lower layer for (a)–(c).

deep ocean, and a ridge that extends either across the island chain or across the entire opening between the marginal sea and the open ocean. Although a simple circulation theory is not available for these configurations (due to either a pressure drop across the topography or bottom pressure torque over a sloping bottom), we make use of the vertical length scale D to interpret the sensitivity of the exchange to these forms of topography.

a. Deep topographic slope

The numerical model is configured with topography that slopes from the perimeter of the island chain into the basin over a width W. To investigate the response of the upper-layer Ekman transport as well as the lower-layer westward geostrophic transport, the shallow ridge to the east of the island chain was removed in this section. The key parameter that measures the importance of topography is the ratio of the gradient in potential vorticity due to the sloping topography and planetary beta, $\alpha = f\Delta h/W\beta H$, where $\Delta h/W$ is the topographic slope, and H is the ocean depth which can be treated as a constant for short topography. For $\alpha \gg 1$, the topography overwhelms planetary beta and closed f/h contours that can isolate the geostrophic flow that comes from the ocean interior are formed around the island chain. We are interested in cases where $\alpha = O(1)$ so that the f/h contours can connect the flat bottom region to the topographic slope region. We note that even for $\alpha \gg 1$ there will be a

narrow ribbon around the edge of the topography along which f/h contours extend from the eastern basin to the western basin. These calculations also include a ridge that extends to 1750-m depth and have a flat bottom at 2000-m depth away from the skirt so that the only difference between these runs is the topographic skirt.

The upper-layer flows are not sensitive to the bottom topography as long as the highest topography is deeper than the vertical scale of the throughflow D. Therefore, we focus on the lower-layer flows which are shown in Fig. 9. For a flat bottom ocean, some of the westward transport is blocked by the ridge and flows northward and southward around the tips of the island chain (Figs. 9a,d). However, the transport around the southern tip is larger than that around the northern tip because of the variation in the Coriolis parameter over the meridional extent of the island. As the topography is introduced around the island chain, the boundary current to the east of the islands becomes more asymmetric because some impinging flow starts to move southward along the f/h contours. If the topography is very weak (Fig. 9b, $\alpha = 2.1$), there are limited f/h contours that connect the marginal sea to the open ocean along the southern tip. The ridges in the gaps form a nearly south–north f/h contour wall across each gap, which blocks the potential vorticity pathways. As the topography increases, more and more f/h contours pass around the southern tip, and some of these even come from the midlatitude of the island chain (Fig. 9c, $\alpha = 5.3$). Therefore, even short

topography of $O(\beta L y H / f_0)$ will create a pathway for water approaching from the east to flow around the southern tip of the island chain and enter the marginal sea. However, the flow in the diffusive boundary layer around the tips is not sensitive to the bottom slope (Fig. 10), so the diffusive balance remains unchanged. Therefore, the flow through the gaps is not affected by the topographic skirt (Fig. 10), because the throughflows are still determined by the diffusive balance. The shift in the transport from the northern tip to the southern tip as the topography increases is evident in Fig. 10.

b. Continental slope and shelf

Many island chains are encircled by a shallow shelf with a continental slope extending to the deep ocean floor. If the shelf were shallow enough, or narrow enough, this may block flow around an island. Our focus is mainly on the circulation around a long island, which is characterized by an overturning cell in the marginal sea and zonal jets at the southern and northern tips of the island in the marginal sea. Similar results were found for a series of smaller islands surrounded by a shelf and slope but the long, single island makes identification of the local shelf-induced overturning cell clearer. To better visualize the overturning flow, we add back the shallow ridge to the east of the island that isolates the upper-layer flow. A set of model calculations were carried out to investigate the dependence of the exchange on the shelf and surrounding topographic skirt. Additional calculations have shown that the circulation is not sensitive to the width of the shelf and the topographic slope, however, it is strongly dependent on the shelf depth. The model is configured with a shelf of 35-km width, whose depth will be varied, around the island and a 100-km-wide topographic skirt around the shelf that slopes linearly from the shelf to the interior ocean floor.

Figure 11 shows the vertically integrated transport streamfunction below the Ekman layer, which reveals the geostrophic flow and the pathway of the return flow. The abrupt transition at the northern boundary of the island is related to the downwelling (upwelling) on the western (eastern) side of the island since we get the transport streamfunction by integrating the zonal velocity from the southern boundary of the domain. In the flat bottom ocean, the impinging Ekman transport on the western side boundary of the island downwells along the boundary and forms a uniform westward return flow (Fig. 11a), which balances the surface eastward Ekman transport and results in a local overturning cell. The northern and southern tip flows are fed by the zonal jets from the marginal sea and get pulled back into the Ekman layer on the eastern side of the island. It is no surprise that the return flow is not affected by the shelf if the shelf is deeper than the upper-layer D because the overturning cell is constrained to the upper layer. However, as the shelf depth decreases and reaches the upper layer the return flow will start to decrease (Fig. 11b). The return flow decreases as the shelf depth gets shallower and more of the flow is steered across the island on the shelf rather than returning to the marginal sea (Fig. 11c). This is evident by the westward flow extending away from the island on the western shelf, which turns north and south and flows around the tips of the island (Figs. 11c,d). As the shelf depth decreases, more return flow
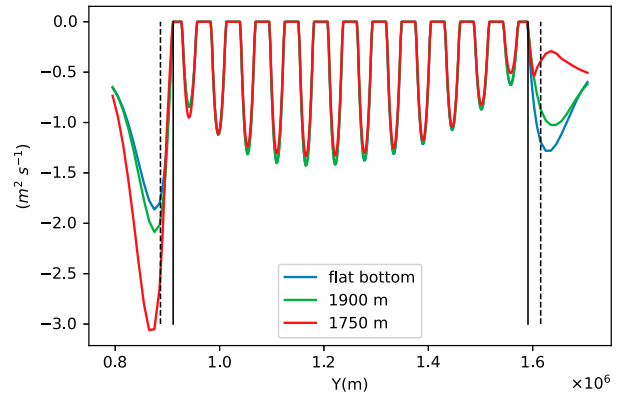

FIG. 10. The vertically integrated zonal velocity at the midlongitude of the island chain in the lower layer for the experiments in Fig. 8. The dashed lines denote the diffusive boundary layer ($l_m = \delta_M^{3/4} L^{1/4}$) from the southern/northern edge (black solid line) of the island chain.

tends to travel northward on the shelf, which gradually increases the northern tip flow and forms an anticyclonic circulation around the island (Fig. 11d). Therefore, the tip flows become more asymmetric and more of the offshore Ekman flow to the east of the island is supported by the northern tip flow. Once on the eastern shelf, the flow turns back toward the island to be drawn into the Ekman layer and continues flowing eastward.

Figure 12 shows the return flow fraction scaled by the Ekman transport within the range of the latitude of the island as a function of the shelf depth scaled by the vertical scale of the upper-layer D (a three-point filter has been applied between 25 and 150 m to suppress small-scale variations). If the shelf is deeper than the upper layer, 90% of the impinging flow returns to the marginal sea. The Ekman transport east of the island is still supported by the zonal tip jets. The return flow decreases as the shelf depth decreases. There is a rapid decrease as the shelf becomes shallower than D. The return flow fraction reduces to about 30% and most of the transport flows around the tips of the island on the shelf. Therefore, the circulation around the ends of the island is gradually supported by the impinging Ekman transport west of the island that flows meridionally on the shelf, which results in weakening tip jets in the marginal sea (Fig. 11). If the shelf depth keeps decreasing, the return flow maintains its weak state with a nearly unchanged transport fraction. However, if the shelf extends to the surface such that the shelf is replaced by a wider island and a surrounding topographic slope, the return flow abruptly increases, and it is very close to the flat bottom ocean (Fig. 12).

c. Ridge across the basin

The topography and island chain alter the surrounding circulation by diverting the exchange around the tips or through the gaps. However, as long as the island chain is far away from the southern and northern boundaries, the total exchange between the marginal sea and the open ocean is not affected by the island chain. Given that the f/h contours strongly steer the flow it seems
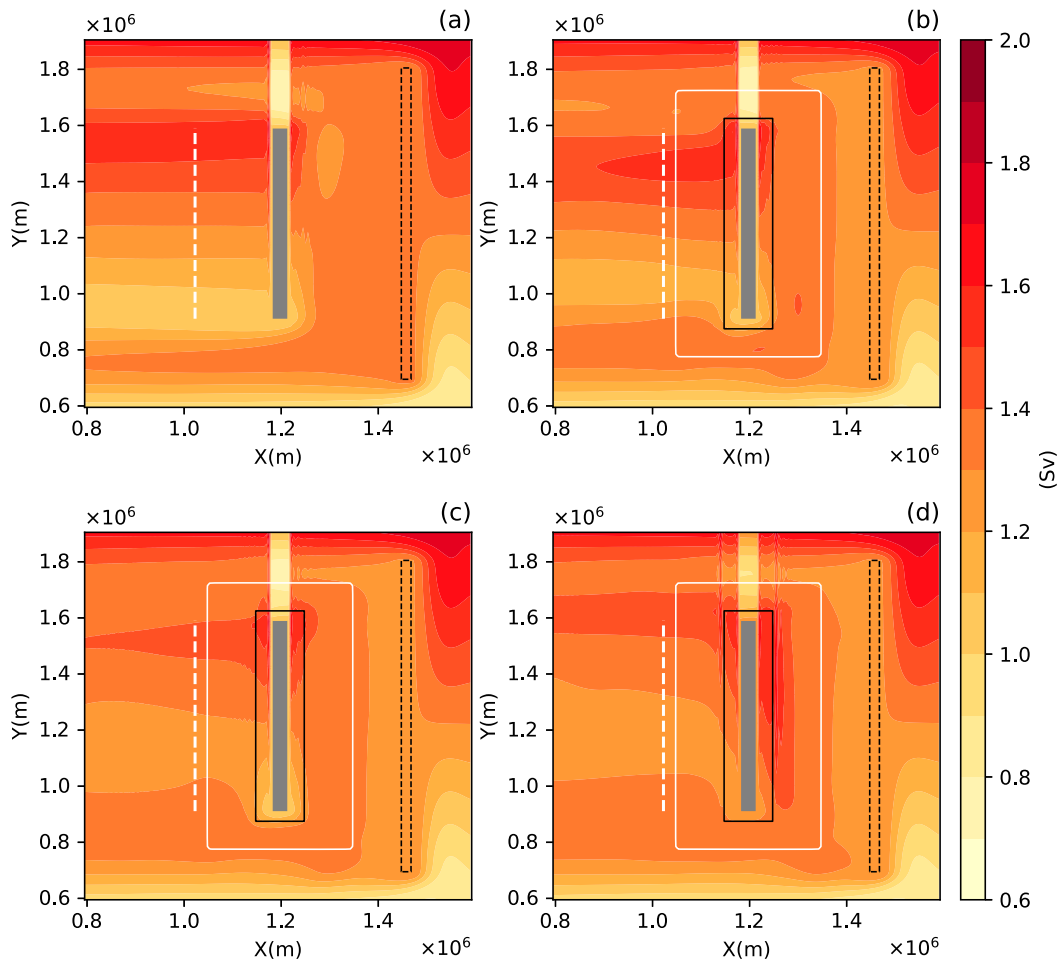
FIG. 11. The vertically integrated transport streamfunction below the Ekman layer for the experiments with a shelf and a topographic slope around a long island. (a) Flat bottom and (b) 250-, (c) 150-, and (d) 25-m depth of the shelf. The solid black (white) line denotes the edge of the shelf (the topographic slope). The dashed white line denotes the section where we calculate the return flow. The dashed black line denotes the shallow ridge.

possible that a tall ridge that extends all the way across the opening between the marginal sea and the open ocean might be effective at blocking or diverting the exchange. Such a shallow ridge could also be populated by islands but we focus here on the ability of just the submerged ridge to block exchange. We now consider a series of calculations in a simplified domain that contains a single narrow ridge that extends from the northern boundary to the southern boundary (Fig. 13). For all cases considered here, the ridge does not penetrate into the Ekman layer so there is always an eastward Ekman flow from the marginal near the surface. If the ridge penetrates into the Ekman layer the Ekman transport will be blocked, which results in two individual overturning cells in the marginal sea and the open ocean.

The offshore Ekman transport lowers the sea surface height (SSH) at the western boundary of the marginal sea. This low-pressure signal propagates cyclonically around the basin as a coastal wave setting up a pressure gradient normal to the boundary. This pressure gradient drives a geostrophic flow below the surface Ekman layer from the open ocean to

the marginal sea. It is this coastal current that supplies the offshore transport that feeds into the Ekman layer (Allen 1976). This is evident in the transport streamfunction calculated between the bottom of the Ekman layer and depth D, shown in Fig. 13a. The flow in the interior is weak and toward the west while most of the transport into the Ekman layer at the western boundary is provided by a boundary current along the southern boundary. There is a similar weak westward flow below depth D, which returns to the eastern basin in a boundary current along the southern boundary Fig. 13d, forming a horizontal recirculation gyre.

The ridge strongly alters the horizontal structure of the exchange flow. If the ridge at the mouth of the marginal sea is deeper than the depth of the upper layer, the upper layer is unchanged and the lower-layer geostrophic flow begins to be blocked. Some of the deep westward flow turns to the south in an inertial boundary layer on the eastern side of the ridge such that the change in planetary vorticity is balanced by an increase in relative vorticity (Fig. 13e). This southward
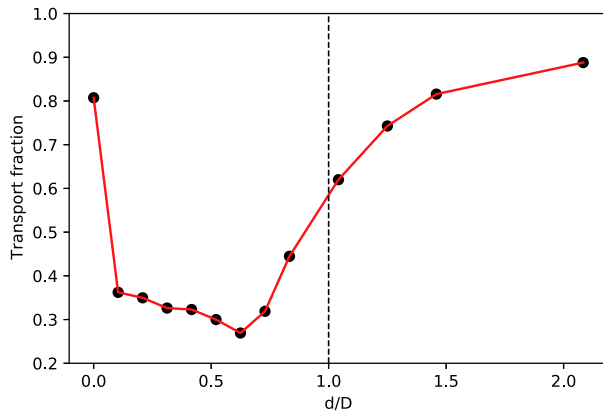
FIG. 12. The return flow scaled by the Ekman transport within the latitude range of the island for the experiments with different depths of the shelf (d) that is scaled by the vertical scale of the upper-layer D.

boundary current flows back to the eastern restoring region along the southern boundary. If the ridge reaches the bottom of the upper layer (Figs. 13b,e), all the deep westward geostrophic flow is blocked, while the flow into the marginal sea in the upper layer remains along the southern boundary.

If the ridge keeps increasing in height so that it is shallower than the vertical scale D, the return flow at the southern mouth of the marginal sea is partly blocked. The deep flow remains fully blocked and forms a cyclonic recirculation gyre, as for the intermediate height ridge. A case where the ridge extends to 30-m depth is shown in Figs. 13c,f. The upper-layer flow in the southern boundary current is now blocked by the ridge. The blocked westward flow will accumulate in the eastern basin, while the surface eastward Ekman transport keeps extracting fluid from the western basin. Therefore, the blocking of return flow leads to a strong zonal SSH gradient above the ridge (Fig. 14a). This SSH gradient will build a meridional flow above the ridge. This flow drives a bottom Ekman layer, which advects water from the eastern basin over the top of the ridge into the western basin. There is also a weak meridional SSH gradient which drives a zonal geostrophic flow into the western basin. In steady state, these two flows balance the surface Ekman flow.

The westward flow on the ridge draws fluid from the eastern basin and lifts the isopycnals on the eastern side of the ridge. The basic response is similar to that found in the interaction of the Ekman layers and lateral boundary, which builds an alongshore baroclinic flow in response to the isopycnal slope (Pedlosky 2013). Therefore, the uplift of the isopycnals on the eastern side of the ridge will bring dense water upward and forms some high potential vorticity (PV) water on the ridge (Fig. 14b). Once the westward flow passes over the ridge, it mixes vertically down to the depth at which the dense water approached the ridge from the east. This produces low-PV water on the western side of the ridge (Fig. 14b), where it is advected nearly zonally to the western boundary by the interior geostrophic flow. Away from the ridge, the zonal overturning circulation remains distributed over the vertical depth scale D, even for the case with a very

shallow ridge (Figs. 13g–i). In summary, if the ridge is deeper than D, the return flow is limited within the southern boundary of the marginal sea, while if the ridge is shallower than D, the return flow is distributed along the ridge and friction in the bottom boundary layer is important.

5. Summary

The exchange between a marginal sea to the west of the open ocean separated by an island chain and/or bottom topography has been explored using a numerical model and an extended island rule theory. Under uniform northward wind stress, there is an eastward surface Ekman transport out of the marginal sea and a westward geostrophic flow into the marginal sea. The results discussed here are linear, so winds to the south would merely reverse the direction of flow.

The island chain between the marginal sea and the open ocean block some of the Ekman transport and create a local overturning cell in the marginal sea. The same amount of transport that was blocked is returned to the open ocean in the form of zonal jets that extend from the northern and southern tips of the island chain to the western boundary. The Ekman transport impinging on the islands results in baroclinic boundary currents with a vertical depth scale $D = (\tau f_0 / \rho_0 N^2 \beta)^{1/3}$ that connect the western and eastern sides of the island. The flow through the gaps is characterized by maximum transport in the middle of the island chain with decreasing transport toward the southern and northern tips of the island chain. An extended island rule theory demonstrates that the flow through the gaps is determined by a diffusive balance between the meridional boundaries and the eastern side boundary of each of the islands. For gaps narrower than the diffusive boundary layer thickness the flow through the archipelago is partially blocked. The degree of blocking is primarily characterized by a single nondimensional number R. In general, fewer and narrow gaps, strong viscosity, and small β will increase blockage. However, many very narrow islands, in which most of the archipelago is open ocean, are also effective at blocking throughflow because friction in the many narrow gaps requires a strong flow around the island chain. Primitive equation model calculations agree well with predictions of the magnitude and distribution of the flow through the archipelago from the theory.

Bottom topography and ridges can also alter the structure of the exchange flows. Shelves around the island have little effect if they are deeper than the vertical length scale D. Shallower shelves can enhance flow through the island chain because some water that downwells along the western side of the island remains trapped on the shelf and flows through the gaps to provide upwelling into the Ekman layer on the eastern side of the island. A deep topographic skirt around the islands creates an effective pathway for barotropic westward geostrophic flows to pass around the southern tip of the island chain into the marginal sea. A ridge that extends all the way across the mouth of the marginal sea plays an important role in the broadscale exchange between the marginal sea and open ocean. For ridges deeper than the vertical length scale D, the eastward Ekman transport is provided primarily by a shallow westward flow along the southern boundary. If the ridge is shallower than this
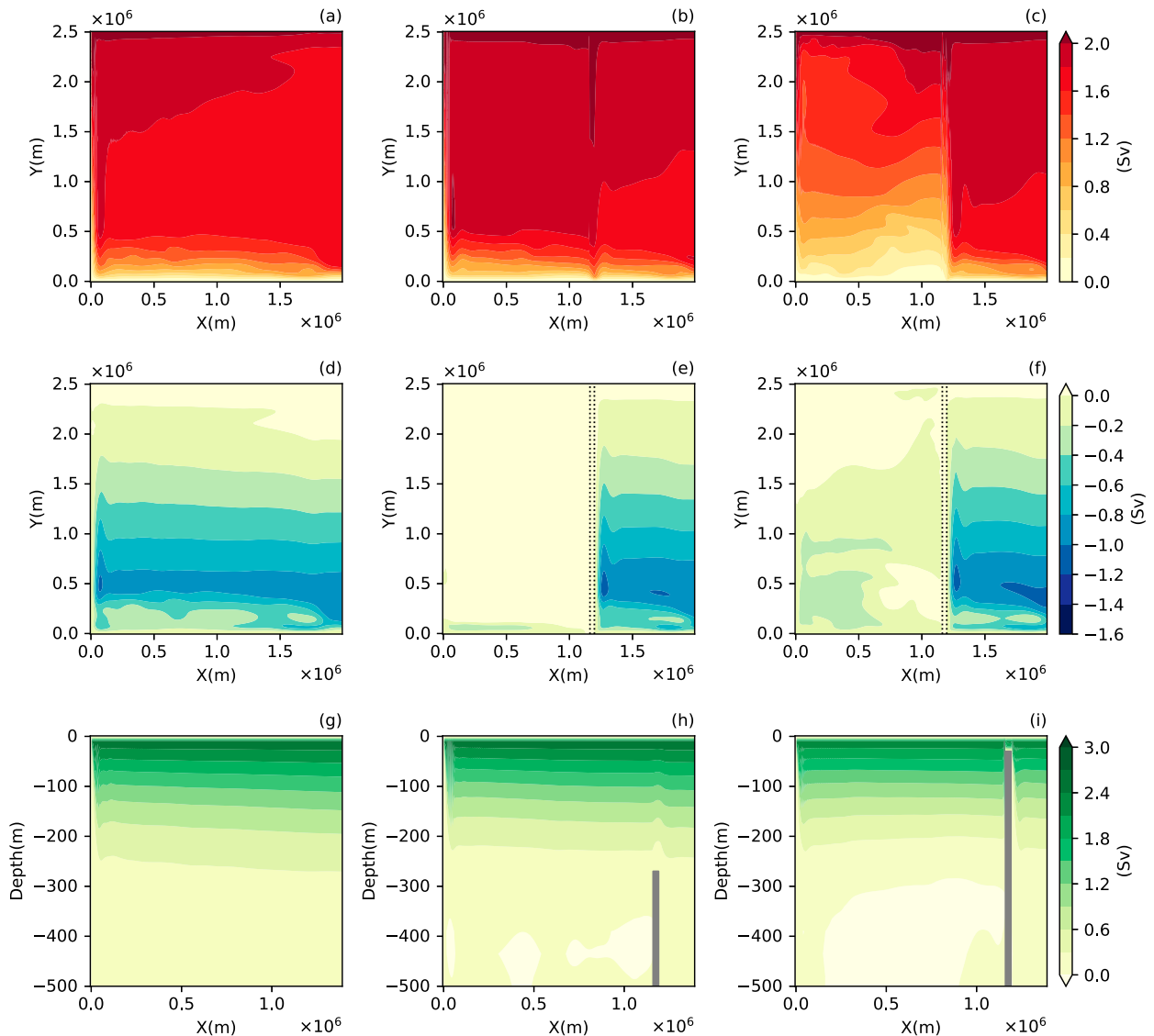
FIG. 13. The vertically integrated streamfunction between the base of the Ekman layer and the upper-layer D for (a) flat bottom, (b) ridge to 270 m, and (c) ridge to 30 m. (d)–(f) The transport streamfunction between depth D and the bottom for the same cases; the dashed lines denote the ridge. (g)–(i) The zonal overturning circulation streamfunction.

vertical scale, the return flow into the marginal sea is distributed all along the ridge. As long as the ridge does not penetrate into the Ekman layer, the total wind-driven exchange between the marginal sea and the open ocean is controlled by the Ekman transport at the ridge. However, the ridge height does impact where waters enter the marginal sea.

A chain of closely spaced islands and/or bottom topography are not very effective at blocking the exchange between marginal seas and the open ocean. The islands may block the exchange locally, and result in a wind-driven overturning cell in the marginal sea, but the pressure signal radiating westward from the island chain forms jets at the northern and southern tips of the island chain. These jets carry the same amount of transport into the open ocean. Ridges are able to block the deep flow, but unless they penetrate into the surface Ekman

layer, they are not able to limit the total exchange. Thus, neither dense island chains nor tall ridges are effective at blocking the net exchange between a marginal sea and the open ocean forced by Ekman transport.

Several strong and simplifying assumptions have been made in order to provide simple, but clarifying, solutions to the question of topographic influences on the wind-driven exchange between marginal seas and the open ocean. For example, the Ekman layer is limited in the top layer (10 m) in the model, which is thin compared to the real ocean. Realistic archipelagos consist of complex, irregularly spaced and shaped islands and ridges, whereas we consider rectangular, homogeneous islands all at the same longitude. The theory developed here is for the time-mean exchange between the marginal sea and the open ocean forced by homogeneous wind stress.
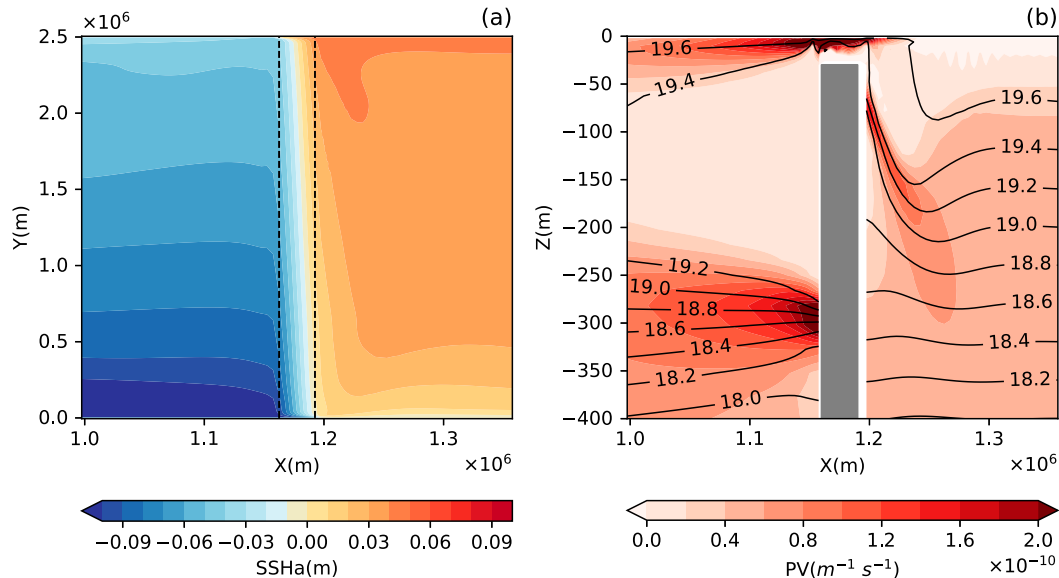
FIG. 14. (a) The sea surface height anomaly for the experiment with 30-m ridge and (b) the vertical section of the potential vorticity (colors) and temperature (black contours) at the midlatitude of the basin. The dashed lines in (a) denote the edge of the ridge.

The influences of time dependence, wind stress curl, and nonlinearities are also of interest.

REFERENCES

Allen, J. S., 1976: Some aspects of the forced wave response of stratified coastal regions. *J. Phys. Oceanogr.*, **6**, 113–119, https://doi.org/10.1175/1520-0485(1976)006<0113:SAOTFW>2.0.CO;2.

Arango, H., and Coauthors, 2011: Development of a hindcast/forecast model for the Philippine Archipelago. *Oceanography*, **24**, 58–69, https://doi.org/10.5670/oceanog.2011.04.

Diansky, N. A., D. V. Stepanov, A. V. Gusev, and V. V. Novotryasov, 2016: Role of wind and thermal forcing in the formation of the water circulation variability in the Japan/East Sea Central Basin in 1958–2006. *Izv. Atmos. Ocean. Phys.*, **52**, 207–216, https://doi.org/10.1134/S0001433816010023.

Fang, G., Y. Wang, Z. Wei, Y. Fang, F. Qiao, and X. Hu, 2009: Interocean circulation and heat and freshwater budgets of the South China Sea based on a numerical model. *Dyn. Atmos. Oceans*, **47**, 55–72, https://doi.org/10.1016/j.dynatmoce.2008.09.003.

Godfrey, J. S., 1989: A Sverdrup model of the depth-integrated flow for the world ocean allowing for island circulations. *Geophys. Astrophys. Fluid Dyn.*, **45**, 89–112, https://doi.org/10.1080/03091928908208894.

Han, W., and Coauthors, 2009: Seasonal surface ocean circulation and dynamics in the Philippine Archipelago region during 2004–2008. *Dyn. Atmos. Oceans*, **47**, 114–137, https://doi.org/10.1016/j.dynatmoce.2008.10.007.

McCreary, J. P., P. K. Kundu, and S.-Y. Chao, 1987: On the dynamics of the California Current system. *J. Mar. Res.*, **45**, 1–32, https://doi.org/10.1357/002224087788400945.

Nan, F., H. Xue, and F. Yu, 2015: Kuroshio intrusion into the South China Sea: A review. *Prog. Oceanogr.*, **137**, 314–333, https://doi.org/10.1016/j.pocean.2014.05.012.

Pedlosky, J., 2013: An inertial model of the interaction of Ekman layers and planetary islands. *J. Phys. Oceanogr.*, **43**, 1398–1406, https://doi.org/10.1175/JPO-D-13-028.1.

——, L. J. Pratt, M. A. Spall, and K. R. Helfrich, 1997: Circulation around islands and ridges. *J. Mar. Res.*, **55**, 1199–1251, https://doi.org/10.1357/0022240973224085.

Pratt, L. J., and J. Pedlosky, 1998: Barotropic circulation around islands with friction. *J. Phys. Oceanogr.*, **28**, 2148–2162, https://doi.org/10.1175/1520-0485(1998)028<2148:BCAIWF>2.0.CO;2.

——, and M. A. Spall, 2003: A porous-medium theory for barotropic flow through ridges and archipelagos. *J. Phys. Oceanogr.*, **33**, 2702–2718, https://doi.org/10.1175/1520-0485(2003)033<2702:APTFBF>2.0.CO;2.

Spall, M. A., 2002: Wind- and buoyancy-forced upper ocean circulation in two-strait marginal seas with application to the Japan/East Sea. *J. Geophys. Res.*, **107**, 3006, https://doi.org/10.1029/2001JC000966.

——, and J. Pedlosky, 2013: Interaction of Ekman layers and islands. *J. Phys. Oceanogr.*, **43**, 1028–1041, https://doi.org/10.1175/JPO-D-12-0159.1.

Stepanov, D. V., N. A. Diansky, and V. V. Fomin, 2018: Eddy energy sources and mesoscale eddies in the Sea of Okhotsk. *Ocean Dyn.*, **68**, 825–845, https://doi.org/10.1007/s10236-018-1167-3.

Suginohara, N., 1982: Coastal upwelling: Onshore-offshore circulation, equatorward coastal jet and poleward undercurrent over a continental shelf-slope. *J. Phys. Oceanogr.*, **12**, 272–284, https://doi.org/10.1175/1520-0485(1982)012<0272:CUOCEC>2.0.CO;2.

Tang, D., I.-H. Ni, F. Müller-Karger, and I. Oh, 2004: Monthly variation of pigment concentrations and seasonal winds in

China's marginal seas. *Hydrobiologia*, **511**, 1–15, https://doi.org/10.1023/B:HYDR.0000014001.43554.6f.

Wajsowicz, R. C., 1996: Flow of a western boundary current through multiple straits: An electrical circuit analogy for the Indonesian throughflow and archipelago. *J. Geophys. Res.*, **101**, 12 295–12 300, https://doi.org/10.1029/95JC02615.

Wu, K., M. Dai, J. Chen, F. Meng, X. Li, Z. Liu, C. Du, and J. Gan, 2015: Dissolved organic carbon in the South China Sea and its exchange with the western Pacific Ocean. *Deep-Sea Res. II*, **122**, 41–51, https://doi.org/10.1016/j.dsr2.2015.06.013.

Yang, H., L. Wu, Z. Chen, and S. Sun, 2017: Selective response of the South China Sea circulation to summer monsoon. *J. Phys. Oceanogr.*, **47**, 1555–1568, https://doi.org/10.1175/JPO-D-16-0288.1.

Yoshida, K., 1980: The coastal undercurrent - A role of longshore scales in coastal upwelling dynamics. *Prog. Oceanogr.*, **9**, 81–131, https://doi.org/10.1016/0079-6611(80)90001-4.